We are IntechOpen, the world's leading publisher of Open Access books Built by scientists, for scientists

4,800
Open access books available

122,000
International authors and editors

135M
Downloads

154
Countries delivered to

Our authors are among the

TOP 1%
most cited scientists

12.2%
Contributors from top 500 universities

CLARIVATE ANALYTICS
BOOK CITATION INDEX
INDEXED

WEB OF SCIENCE™

Selection of our books indexed in the Book Citation Index
in Web of Science™ Core Collection (BKCI)

Interested in publishing with us?
Contact book.department@intechopen.com

Numbers displayed above are based on latest data collected.
For more information visit www.intechopen.com

Boundary Element Mathematical Modelling and Boundary Element Numerical Techniques for Optimization of Micropolar Thermoviscoelastic Problems in Solid Deformable Bodies

Mohamed Abdelsabour Fahmy

Abstract

The main objective of this chapter is to introduce a new theory called three-temperature nonlinear generalized micropolar thermoviscoelasticity. Because of strong nonlinearity of simulation and optimization problems associated with this theory, the numerical solutions for problems related with the proposed theory are always very difficult and require the development of new numerical techniques. So, we propose a new boundary element technique for simulation and optimization of such problems based on genetic algorithm (GA), free form deformation (FFD) method and nonuniform rational B-spline curve (NURBS) as the shape optimization technique. In the formulation of the considered problem, the profiles of the considered objects are determined by FFD method, where the FFD control points positions are treated as genes, and then the chromosomes profiles are defined with the genes sequence. The population is founded by a number of individuals (chromosomes), where the objective functions of individuals are determined by the boundary element method (BEM). The numerical results verify the validity and accuracy of our proposed technique.

Keywords: boundary element modeling, simulation, optimization, three-temperature, nonlinear generalized micropolar thermoviscoelasticity, solid deformable bodies

1. Introduction

The classical thermo-elasticity (CTE) theory which was introduced by Duhamel [1] and Neumann [2] characterized the strain-temperature gradients equations in an elastic body, but it has two shortcomings contrary to physical observations: First, the heat conduction equation of this theory does not include any elastic terms. Second, the heat conduction equation is of a parabolic type predicting infinite speeds of thermal waves. Biot [3] developed the classical coupled thermo-elasticity (CCTE) theory to overcome the first shortcoming in CTE. However, both theories

share the second shortcoming. So, several generalized thermoelasticity theories that predict finite speeds of propagation for heat waves have been developed such as extended thermo-elasticity (ETE) theory of Lord and Shulman [4], temperature-rate-dependent thermo-elasticity (TRDTE) theory of Green and Lindsay [5], three linear generalized thermoelasticity theories (type I, II and III) of Green and Naghdi [6, 7], low-temperature thermoelasticity (LTTE) model of Hetnarski and Ignaczak [8], the dual phase-lag (DPL) heat conduction equation of Tzou [9, 10] which has been developed taking into consideration the phonons-electrons interactions to obtain dual phase-lag thermoelasticity (DPLTE) [11, 12], and three-phase-lag thermoelasticity (TPLTE) model of Choudhuri [13] who takes into consideration the phase-lags of heat flux, temperature gradient and thermal displacement gradient. Chen and Gurtin [14], introduced the theory of two-temperatures (conductive temperature and thermodynamic temperature) heat conduction in the context of elastic bodies, then Youssef [15] extended this theory to generalized thermoelasticity. Fahmy [16] introduced three-temperature nonlinear generalized micropolar-magneto-thermoelasticity theory and developed a new boundary element technique for Modeling and Simulation of complex problems associated with this theory. Theory of micropolar elasticity [17, 18] has been developed for studying the mechanical behavior of polymers and elastomers and applied in many applications [19–24]. Then, Eringen [25] and Nowacki [26] extended it to micropolar thermoelasticity, and then implemented in various applications [27–29]. Because of strong nonlinearity of three-temperatures radiative heat conduction equations, the numerical solution and simulation of such problems are always difficult and require the development of new numerical schemes [30, 31]. In comparison with other numerical methods [32–34], the boundary element method has been successfully applied and performed for solving various applications [35–60]. The boundary element technique has been formulated in the context of micropolar thermoelasticity by Sladek and Sladek [61–63] and Huang and Liang [64]. Through the current paper, the term three-temperatures introduced for the first time in the field of nonlinear generalized micropolar thermoviscoelasticity. Recently, evolutionary algorithms [65, 66] have received much attention of researchers. The genetic algorithm (GA) can deal with the multi-objective and complex shapes problems. Also, it could reach an optimal solution with highly reduced computational cost.

The main aim of this article is to introduce a new theory called nonlinear generalized micropolar thermoviscoelasticity involving three temperatures. Because of strong nonlinearity, it is very difficult to solve the problems related to this theory analytically. Therefore, we propose a new boundary element model for simulation and optimization of three temperatures nonlinear generalized micropolar thermoviscoelastic problems associated with this theory. The genetic algorithm (GA) was implemented based on free form deformation (FFD) technique and nonuniform rational B-spline (NURBS) curve as an optimization technique for the considered problems. The numerical results demonstrate the validity and accuracy of our proposed model.

2. Formulation of the problem

The governing equations for three-temperature anisotropic generalized micropolar thermoviscoelasticity problems can be expressed as [58]

$$\sigma_{ij,j} + \rho F_i = \rho \ddot{u}_i \tag{1}$$

$$m_{ij,j} + \varepsilon_{ijk}\sigma_{jk} + \rho M_i = J\rho\ddot{\omega}_i \tag{2}$$

where

$$\sigma_{ij} = C_{ijkl} \divideontimes e\delta_{ij} + \breve{\alpha}(u_{j,i} - \varepsilon_{ijk}\omega_k) - \beta_{ij}T_\alpha \left(C_{ijkl} = C_{klij} = C_{jikl}, \beta_{ij} = \beta_{ji}\right) \tag{3}$$

$$m_{ij} = \alpha\,\omega_{k,k}\delta_{ij} + \overline{\alpha}\omega_{i,j} + \overline{\overline{\alpha}}\omega_{j,i} \tag{4}$$

$$\epsilon_{ij} = \varepsilon_{ij} - \varepsilon_{ijk}(r_k - \omega_k), \varepsilon_{ij} = \frac{1}{2}\left(u_{i,j} + u_{j,i}\right), r_i = \frac{1}{2}\varepsilon_{ikl}u_{l,k} \tag{5}$$

The two-dimension three-temperature (2D-3T) radiative heat conduction equations can be expressed as [53]

$$c_e\frac{\partial T_e(r,\tau)}{\partial\tau} - \frac{1}{\rho}\nabla[\mathbb{K}_e\nabla T_e(r,\tau)] = -\mathbb{W}_{ei}(T_e - T_i) - \mathbb{W}_{ep}(T_e - T_p) \tag{6}$$

$$c_i\frac{\partial T_i(r,\tau)}{\partial\tau} - \frac{1}{\rho}\nabla[\mathbb{K}_i\nabla T_i(r,\tau)] = \mathbb{W}_{ei}(T_e - T_i) \tag{7}$$

$$\frac{4}{\rho}c_pT_p^3\frac{\partial T_p(r,\tau)}{\partial\tau} - \frac{1}{\rho}\nabla\left[\mathbb{K}_p\nabla T_p(r,\tau)\right] = \mathbb{W}_{ep}(T_e - T_p) \tag{8}$$

3. A new mathematical modelling of nonlinear generalized micropolar thermoviscoelasticity problem

With reference to a Cartesian coordinate system (x_1, x_2, x_3), we consider an anisotropic micropolar thermoviscoelastic structure occupies the region R which bounded by a closed surface S, and $S_i(i = 1, 2, 3, 4)$ denotes subsets of S such that $S_1 + S_2 = S_3 + S_4 = S$.

3.1 BEM simulation for temperature field

The 2D-3T radiative heat conduction Eqs. (6)–(8) can be expressed as [53]

$$\nabla[\mathbb{K}_\alpha\nabla T_\alpha(r,\tau)] + \overline{\mathbb{W}}(r,\tau) = c_\alpha\rho\delta_1\frac{\partial T_\alpha(r,\tau)}{\partial\tau} \tag{9}$$

where

$$\overline{\mathbb{W}}(r,\tau) = \begin{cases} -\rho\,\mathbb{W}_{ei}(T_e - T_i) - \rho\,\mathbb{W}_{ep}(T_e - T_p), \alpha = e, \delta_1 = 1 \\ \rho\,\mathbb{W}_{ei}(T_e - T_i), \alpha = i, \delta_1 = 1 \\ \rho\,\mathbb{W}_{ep}(T_e - T_p), \alpha = p, \delta_1 = \frac{4}{\rho}T_p^3 \end{cases} \tag{10}$$

and

$$\mathbb{W}_{ei} = \rho\mathbb{A}_{ei}T_e^{-2/3}, \mathbb{W}_{ep} = \rho\mathbb{A}_{ep}T_e^{-1/2}, \mathbb{K}_\alpha = \mathbb{A}_\alpha T_\alpha^{5/2}, \alpha = e, i, \mathbb{K}_p = \mathbb{A}_p T_p^{3+\mathbb{B}} \tag{11}$$

where parameters c_α, $\mathbb{A}_\alpha(\alpha = e, i, p)$, $\mathbb{B}$, $\mathbb{A}_{ei}$, $\mathbb{A}_{ep}$ are constant inside each subdomain, but they are discontinuous on the interfaces between subdomains.

The total energy of unit mass can be described by

$$P = P_e + P_i + P_p, P_e = c_e T_e, P_i = c_i T_i, P_p = \frac{1}{\rho} c_P T_P^4 \tag{12}$$

Initial and boundary conditions can be written as

$$T_\alpha(x, y, 0) = T_\alpha^0(x, y) = g_1(x, \tau) \tag{13}$$

$$\mathbb{K}_\alpha \frac{\partial T_\alpha}{\partial n}\bigg|_{\Gamma_1} = 0, \alpha = e, i, T_p\big|_{\Gamma_1} = g_2(x, \tau) \tag{14}$$

$$\mathbb{K}_\alpha \frac{\partial T_\alpha}{\partial n}\bigg|_{\Gamma_2} = 0, \alpha = e, i, p \tag{15}$$

we use the time-dependent fundamental solution which is a solution of the following differential equation

$$D\nabla^2 T_\alpha + \frac{\partial T_\alpha^*}{\partial n} = -\delta(r - p_i)\delta(\tau - r), D = \frac{\mathbb{K}_\alpha}{\rho c} \tag{16}$$

In which the points p_i are the singularities, where the temperatures are not defined there. Singular integrals are those whose kernels are not defined at the singularities on the integration domain R. They are defined by eliminating a small space including the singularity, and obtaining the limit when this small space tends to zero [40, 46].

The boundary integral equation corresponding to our considered heat conduction can be written as in Fahmy [46–48] as follows

$$CT_\alpha = \frac{D}{\mathbb{K}_\alpha} \int_O^\tau \int_S [T_\alpha q^* - T_\alpha^* q] dS \, d\tau + \frac{D}{\mathbb{K}_\alpha} \int_O^\tau \int_R bT_\alpha^* dR \, d\tau + \int_R T_\alpha^i T_\alpha^* \big|_{\tau=0} \tag{17}$$

which can be expressed in the following form [53].

$$CT_\alpha = \int_S [T_\alpha q^* - T_\alpha^* q] \, dS - \int_R \frac{\mathbb{K}_\alpha}{D} \frac{\partial T_\alpha^*}{\partial \tau} T_\alpha \, dR \tag{18}$$

The time derivative of temperature T_α can be approximated as

$$\frac{\partial T_\alpha}{\partial \tau} \cong \sum_{j=1}^N f^j(r)^j a^j(\tau). \tag{19}$$

where $f^j(r)$ and $a^j(\tau)$ are known functions and unknown coefficients, respectively.

Also, we assume that $\widehat{T}_\alpha^j$ is a solution of

$$\nabla^2 \widehat{T}_\alpha^j = f^j \tag{20}$$

Thus, Eq. (18) results in the following boundary integral equation [53]

$$C T_\alpha = \int_S [T_\alpha q^* - T_\alpha^* q] \, dS + \sum_{j=1}^N a^j(\tau) D^{-1} \left(C\widehat{T}_\alpha^j - \int_S \left[T_\alpha^j q^* - \widehat{q}^j T_\alpha^* \right] dS \right) \tag{21}$$

where

$$\widehat{q}^j = -\mathbb{K}_\alpha \frac{\partial \widehat{T}_\alpha^j}{\partial n} \tag{22}$$

and

$$a^j(\tau) = \sum_{i=1}^{N} f_{ji}^{-1} \frac{\partial T(r_i, \tau)}{\partial \tau} \tag{23}$$

In which the entries of f_{ji}^{-1} are the coefficients of F^{-1} which described in [34].

$$\{F\}_{ji} = f^j(r_i) \tag{24}$$

The boundary integral discretization scheme has been applied to (21) with the use of (23), we get [53]

$$C\,\dot{T}_\alpha + H\,T_\alpha = G\,Q \tag{25}$$

where T_α and Q are temperature, heat flux vectors and internal heat generation vectors, respectively.

The diffusion matrix can be defined as

$$C = -\left[H\,\widehat{T}_\alpha - G\,\widehat{Q}\right]F^{-1}D^{-1} \tag{26}$$

with

$$\left\{\widehat{T}\right\}_{ij} = \widehat{T}^j(x_i) \tag{27}$$

$$\left\{\widehat{Q}\right\}_{ij} = \widehat{q}^j(x_i) \tag{28}$$

For solving (25) numerically, we interpolate the functions T_α and q as

$$T_\alpha = (1-\theta)T_\alpha^m + \theta\,T_\alpha^{m+1} \tag{29}$$

$$q = (1-\theta)q^m + \theta\,q^{m+1} \tag{30}$$

where $0 \le \theta = \frac{\tau - \tau^m}{\tau^{m+1} - \tau^m} \le 1$.

The time derivative of (29) can be expressed as

$$\dot{T}_\alpha = \frac{dT_\alpha}{d\theta}\frac{d\theta}{d\tau} = \frac{T_\alpha^{m+1} - T_\alpha^m}{\tau^{m+1} - \tau^m} = \frac{T_\alpha^{m+1} - T_\alpha^m}{\Delta\tau^m} \tag{31}$$

By substituting from Eqs. (29)–(31) into Eq. (25), we obtain

$$\left(\frac{C}{\Delta\tau^m} + \theta H\right)T_\alpha^{m+1} - \theta GQ^{m+1} = \left(\frac{C}{\Delta\tau^m} - (1-\theta)H\right)T_\alpha^m + (1-\theta)GQ^m \tag{32}$$

Making use of initial conditions and boundary conditions at $\Delta\tau^m$ and considering the previous time step solution as initial values for next step, we get

$$aX = b \tag{33}$$

The Adaptive Smoothing and Prolongation Algebraic Multigrid (aSP-AMG) method, which uses an adaptive Factorized Sparse Approximate Inverse (aFSAI) [67] preconditioner as high performance technique that has been implemented efficiently in Matlab (R2018a) for solving the resulting simultaneous linear algebraic systems (33).

3.2 BEM simulation for micropolar thermoviscoelastic fields

According to the weighted residual method, we can write the differential Eqs. (1) and (2) in the following integral form

$$\int_R (\sigma_{ij,j} + U_i)u_i^* \, dR = 0 \tag{34}$$

$$\int_R (m_{ij,j} + \varepsilon_{ijk}\sigma_{jk} + V_i)\omega_i^* \, dR = 0 \tag{35}$$

where

$$U_i = \rho F_i - \rho\ddot{u}_i, V_i = \rho(M_i - J\ddot{\omega}_i) \tag{36}$$

The boundary conditions are

$$u_i = \bar{u}_i \text{ on } S_1 \tag{37}$$

$$\lambda_i = \sigma_{ij}n_j = \bar{\lambda}_i \text{ on } S_2 \tag{38}$$

$$\omega_i = \bar{\omega}_i \text{ on } S_3 \tag{39}$$

$$\mu_i = m_{ij}n_j = \bar{\mu}_i \text{ on } S_4 \tag{40}$$

By integrating by parts the first term of Eqs. (34) and (35), we obtain

$$-\int_R \sigma_{ij}u_{i,j}^* \, dR + \int_R U_iu_i^* \, dR = -\int_{S_2} \lambda_iu_i^* \, dS \tag{41}$$

$$-\int_R m_{ij}\omega_{i,j}^* \, dR + \int_R \varepsilon_{ijk}\sigma_{jk}\omega_i^* \, dR + \int_R V_i\omega_i^* \, dR = -\int_{S_4} \mu_i\omega_i^* \, dS \tag{42}$$

On the basis of Huang and Liang [64], we can write

$$-\int_R \sigma_{ij,j}u_i^* \, dR + \int_R (m_{ij,j} + \varepsilon_{ijk}\sigma_{jk})\omega_i^* \, dR + \int_R U_iu_i^* \, dR + \int_R V_i\omega_i^* \, dR$$
$$= \int_{S_2} (\lambda_i - \bar{\lambda}_i)u_i^* \, dS + \int_{S_1} (\bar{u}_i - u_i)\lambda_i^* \, dS + \int_{S_4} (\mu_i - \bar{\mu}_i)\omega_i^* \, dS + \int_{S_3} (\bar{\omega}_i - \omega_i)\mu_i^* \, dS \tag{43}$$

By integrating by parts, the left-hand side of (43) can be written as

$$-\int_R \sigma_{ij}\varepsilon_{ij}^* \, dR - \int_R m_{ij,j}\omega_{i,j}^* \, dR + \int_R U_iu_i^* \, dR + \int_R V_i\omega_i^* \, dR$$
$$= -\int_{S_2} \bar{\lambda}_i\, u_i^* \, dS - \int_{S_1} \lambda_iu_i^* \, dS + \int_{S_1} (\bar{u}_i - u_i)\lambda_i^* \, dS - \int_{S_4} \bar{\mu}_i\omega_i^* \, dS - \int_{S_3} \mu_i\omega_i^* \, dS$$
$$+ \int_{S_3} (\bar{\omega}_i - \omega_i)\mu_i^* \, dS \tag{44}$$

According to Eringen [68], the elastic and couple stresses can be written in the following form

$$\sigma_{ij} = \mathbb{A}_{ijkl}\varepsilon_{kl}, \quad m_{ij} = \mathbb{B}_{ijkl}\omega_{k,l} \tag{45}$$

where $\mathbb{A}_{ijkl} = \mathbb{A}_{klij}$ and $\mathbb{B}_{ijkl} = \mathbb{B}_{klij}$ as shown in [68].

Hence, Eq. (44) can be re-expressed as [53]

$$
\begin{aligned}
&-\int_R \sigma_{ij}^* \varepsilon_{ij} \, dR - \int_R m_{ij,j}^* \omega_{i,j} \, dR + \int_R U_i u_i^* \, dR + \int_R V_i \omega_i^* \, dR \\
&= -\int_{S_2} \overline{\lambda}_i \, u_i^* \, dS - \int_{S_1} \lambda_i u_i^* \, dS + \int_{S_1} (\overline{u}_i - u_i) \lambda_i^* \, dS - \int_{S_4} \overline{\mu}_i \omega_i^* \, dS - \int_{S_3} \mu_i \omega_i^* \, dS \\
&\quad + \int_{S_3} (\overline{\omega}_i - \omega_i) \mu_i^* \, dS
\end{aligned}
\tag{46}
$$

By applying integration by parts again, the left-hand side of (46) can be written as [53]

$$
\begin{aligned}
\int_R \sigma_{ij,j}^* u_i \, dR + \int_R \left(m_{ij,j}^* + \varepsilon_{ijk}\sigma_{jk}^* \right) \omega_i \, dR &= -\int_S u_i^* \lambda_i \, dS - \int_S \omega_i^* \mu_i \, dS + \int_S \lambda_i^* u_i \, dS \\
&\quad + \int_S \mu_i^* \omega_i \, dS
\end{aligned}
\tag{47}
$$

The obtained weighting functions for $U_i = \Delta^n$ and $V_i = 0$ along e_l were first used as follows:

$$\sigma_{lj,j}^* + \Delta^n e_l = 0 \tag{48}$$

$$m_{ij,j}^* + \varepsilon_{ijk}\sigma_{jk}^* = 0 \tag{49}$$

According to Dragos [69], the fundamental solutions can be written as

$$u_i^* = u_{li}^* e_l, \quad \omega_i^* = \omega_{li}^* e_l, \quad \lambda_i^* = \lambda_{li}^* e_l, \quad \mu_i^* = \mu_{li}^* e_l, \tag{50}$$

The obtained weighting functions for $U_i = 0$ and $V_i = \Delta^n$ along e_l were next used as follows:

$$\sigma_{ij,j}^{**} = 0 \tag{51}$$

$$m_{lj,j}^{**} + \varepsilon_{ljk}\sigma_{jk}^{**} + \Delta^n e_l = 0 \tag{52}$$

The fundamental solutions that have been obtained analytically by Dragos [69] can be written as

$$u_i^* = u_{li}^{**} e_l, \quad \omega_i^* = \omega_{li}^{**} e_l, \quad \lambda_i^* = \lambda_{li}^{**} e_l, \quad \mu_i^* = \mu_{li}^{**} e_l, \tag{53}$$

Using the above two sets of weighting functions into (47) we have

$$C_{li}^n u_i^n = -\int_S \lambda_{li}^* u_i dS - \int_S \mu_{li}^* \omega_i dS + \int_S u_{li}^* \lambda_i \, dS + \int_S \omega_{li}^* \mu_i \, dS \tag{54}$$

$$C_{li}^n \omega_i^n = -\int_S \lambda_{li}^{**} u_i dS - \int_S \mu_{li}^{**} \omega_i dS + \int_S u_{li}^{**} \lambda_i \, dS + \int_S \omega_{li}^{**} \mu_i \, dS \tag{55}$$

Thus, we can write

$$C^n \mathbb{q}^n = -\int_S \mathbb{p}^* \mathbb{q} dS + \int_S \mathbb{q}^* \mathbb{p} dS \qquad (56)$$

where

$$C^n = \begin{bmatrix} C_{11} & C_{12} & 0 \\ C_{21} & C_{22} & 0 \\ 0 & 0 & 0 \end{bmatrix}, \mathbb{q}^* = \begin{bmatrix} u_{11}^* & u_{12}^* & \omega_{13}^* \\ u_{21}^* & u_{22}^* & \omega_{23}^* \\ u_{31}^{**} & u_{32}^{**} & \omega_{33}^{**} \end{bmatrix}, \mathbb{p}^* = \begin{bmatrix} \lambda_{11}^* & \lambda_{12}^* & \mu_{13}^* \\ \lambda_{21}^* & \lambda_{22}^* & \mu_{23}^* \\ \lambda_{31}^{**} & \lambda_{32}^{**} & \mu_{33}^{**} \end{bmatrix},$$

$$\mathbb{q} = \begin{bmatrix} u_1 \\ u_2 \\ \omega_3 \end{bmatrix}, \mathbb{p} = \begin{bmatrix} \lambda_1 \\ \lambda_2 \\ \mu_3 \end{bmatrix}$$

In order to solve (56) numerically, we construct the following functions

$$\mathbb{q} = \psi \, \mathbb{q}^j, \mathbb{p} = \psi \, \mathbb{p}^j \qquad (57)$$

substituting above functions into (56) and discretizing the boundary, we obtain

$$C^n \mathbb{q}^n = \sum_{j=1}^{N_e} \left[-\int_{\Gamma_j} \mathbb{p}^* \psi \, d\Gamma \right] \mathbb{q}^j + \sum_{j=1}^{N_e} \left[\int_{\Gamma_j} \mathbb{q}^* \psi \, d\Gamma \right] \mathbb{p}^j \qquad (58)$$

Equation after integration may be expressed as

$$C^i \mathbb{q}^i = -\sum_{j=1}^{N_e} \widehat{\mathbb{H}}^{ij} \mathbb{q}^j + \sum_{j=1}^{N_e} \widehat{\mathbb{G}}^{ij} \mathbb{p}^j \qquad (59)$$

which can be expressed as

$$\sum_{j=1}^{N_e} \mathbb{H}^{ij} \mathbb{q}^j = \sum_{j=1}^{N_e} \widehat{\mathbb{G}}^{ij} \mathbb{p}^j \qquad (60)$$

where

$$\mathbb{H}^{ij} = \begin{cases} \widehat{\mathbb{H}}^{ij} & \text{if } i \neq j \\ \widehat{\mathbb{H}}^{ij} + C^i & \text{if } i = j \end{cases} \qquad (61)$$

Thus, we can write the following system of matrix equation as

$$\mathbb{H}\mathbb{Q} = \mathbb{G}\mathbb{P} \qquad (62)$$

Hence, we get the following system of linear algebraic equations

$$\mathbb{A}\,\mathbb{X} = \mathbb{B} \qquad (63)$$

4. A new boundary element technique for simulation and optimization of solid deformable bodies under different loads

In order to solve (63), we apply adaptive smoothing and prolongation algebraic multigrid (aSP-AMG) based on adaptive Factorized Sparse Approximate Inverse

(aFSAI) as described in [67] for solving the resulting simultaneous linear algebraic system (63) in Matlab (R2018a).

B-spline basis functions are used as weights in the same manner as Bézier basis functions. Spline curves can be expressed in terms of $k -$ order B-spline basis function. All B-spline basis functions are assumed to have their domain on [0,1]. B-splines basis functions are a more general type of curve than Bezier curves, where each control point P_i of $i + 1$ control points $(P_0, P_1, P_2, \dots, P_i)$ is connected with a basis function $N_{i,k}$, the knots are the points that subdivide the domain [0,1] into knot spans. Also, each B-spline basis function is non-zero on the entire interval.

The efficiency of our numerical modeling technique has been improved using a nonuniform rational B-spline curve (NURBS) to decrease the computation time and model optimized boundary where it reduces the number of control points and provides the flexibility to design a large variety of shapes.

The considered NURBS can be defined as follows

$$C(t) = \frac{\sum_{i=0}^{n} N_{i,o}(t)\varpi_i P_i}{\sum_{i=0}^{n} N_{i,o}(t)\varpi_i} \tag{64}$$

where $N_{i,o}(t)$ and ϖ_i are the B-spline basis functions of order o and the weights of control points P_i, respectively.

The genetic algorithm greatly reduces computing time and computer memory of achieving an optimum solution, so, it can be used for solving multi-objective problems without needing to calculate the sensitivities. The profiles of the considered objects are represented based on the free form deformation (FFD) technique, where the FFD control points are considered as the genes and then the profiles of chromosomes are defined by the sequence of genes. The population is constructed by many individuals (chromosomes), where the fitness functions are evaluated by using the BEM.

Two criteria can be implemented during shape optimization of the solid bodies [70]

I. The minimum global compliance:

$$\mathcal{F} = \frac{1}{2}\int_S (\lambda \cdot u)\, dS \tag{65}$$

II. The minimum boundary equivalent stresses

$$\mathcal{F} = \int_S \left(\frac{\sigma_{ij}}{\sigma_0}\right)^n dS \tag{66}$$

σ_{ij}, σ_0 and n are equivalent boundary stresses, reference stress and natural number, respectively, where the greater value of n increases the speed of convergence of the functional (66). By minimizing the functional (66) σ_{ij} are closer to σ_0.

In order to find the optimal boundary conditions for temperature the following functional can be applied

$$\mathcal{F} = \int_S \left(\frac{u}{u_0}\right)^n dS \tag{67}$$

where u and u_0 are boundary displacement and reference displacement, respectively. Minimization of the functional (67) reduces displacements on the selected part of the boundary.

In order to identify unknown inner boundary, we use the following functional

$$\mathcal{F} = \delta \sum_{k=1}^{M} \left(u^k - \widehat{u}^k \right) + \eta \sum_{l=1}^{N} \left(T^l - \widehat{T}^l \right) \tag{68}$$

where $\widehat{u}^k$ and $\widehat{T}^l$ are measured displacements and temperatures in boundary points k and l respectively, u^k and T^l are computed displacements and temperatures in boundary points k and l respectively, δ and η are weight coefficients, and M and N are numbers of sensors.

5. Numerical examples and discussion of results

For illustration of the theoretical results of our proposed technique from the preceding sections, two numerical examples are analyzed below. The first example is the cantilever beam with inferior corner load, the second is the Michell-type structure, where the material has the following physical data [58]:

The elasticity tensor

$$C_{ijkl} = \begin{pmatrix} 60.23 & 18.67 & 18.96 & -7.69 & 15.60 & -25.28 \\ 18.67 & 21.26 & 9.36 & -3.74 & 4.21 & -8.47 \\ 18.96 & 9.36 & 47.04 & -8.82 & 15.28 & -8.31 \\ -7.69 & -3.74 & -8.82 & 10.18 & -9.54 & 5.69 \\ 15.60 & 4.21 & 15.28 & -9.54 & 21.19 & -8.54 \\ -25.28 & -8.47 & -8.31 & 5.69 & -8.54 & 20.75 \end{pmatrix} \tag{69}$$

p = 25 MPa, and $\Delta t = 0.0006$ s.

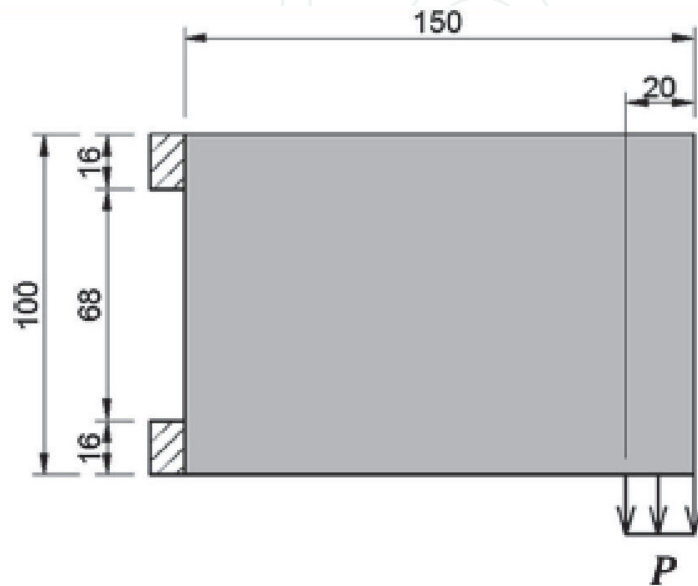**Example 1.** Cantilever beam structure.

Figure 1.
Cantilever beam structure geometry.

As a practical example, the proposed algorithm is applied on the cantilever beam with inferior corner load P = 100 N/mm. The geometry of the cantilever beam is illustrated in **Figure 1**. The initial boundary mesh of the cantilever beam composed of 14 quadratic elements is also illustrated in **Figure 2**. The BEM grid is composed of 76 nodes along x direction and 51 nodes along y direction. These mesh parameters were obtained after convergence analysis. In the process of optimization, the cantilever beam structure optimization results are presented in **Figure 3** from initial to final structure for different iterations.

The present measured boundary element method (BEM) optimization results of the first example are compared in **Figure 4** with measured finite difference method (FDM) optimization results obtained by Itzá et al. [71] and measured finite element method (FEM) optimization results obtained using the software package COMSOL Multiphysics, version 5.4. It is clear from this figure that the BEM results obtained by the proposed technique are in excellent agreement with the FDM results [71] and FEM results of the COMSOL Multiphysics.

Table 1 shows that our proposed BEM modeling of cantilever beam with inferior corner load drastically reduces the manpower needed for modeling and computer resources needed for the calculation in comparison with the calculated results based on the FDM and FEM.

Example 2. Michell-type structure.

As application example, we use a beam with a mid-span load (P = 100 N/mm) (Michell-type structure) as shown in **Figure 5**. The initial boundary mesh of the Michell-type structure composed of 40 quadratic discontinuous elements is also

Figure 2.
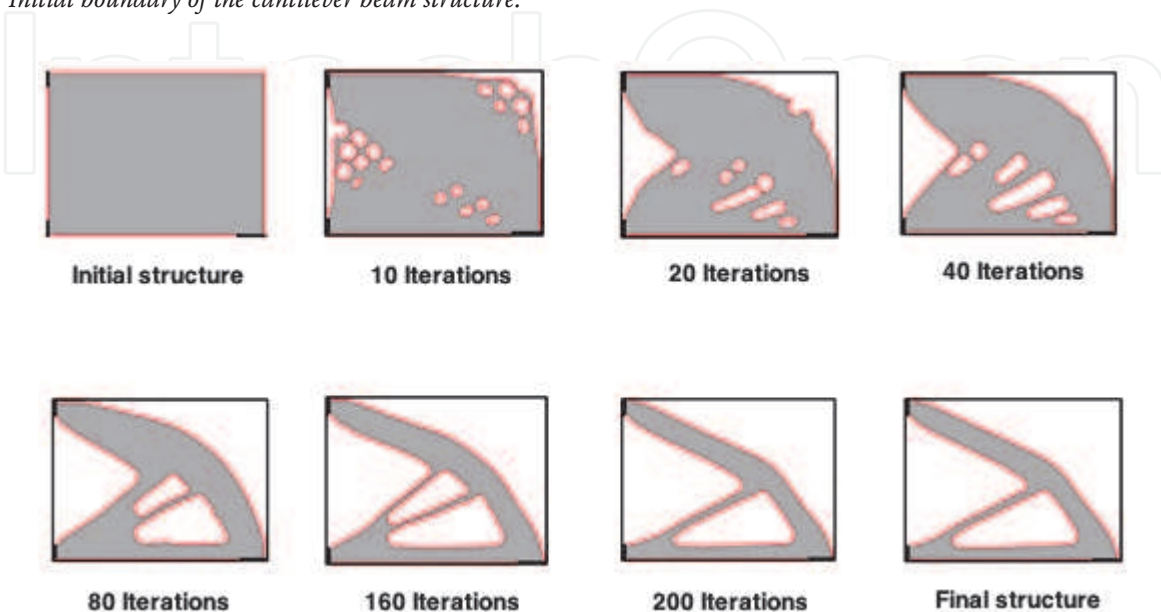*Initial boundary of the cantilever beam structure.*

Figure 3.
Cantilever beam optimization process from initial to final structure for different iterations.
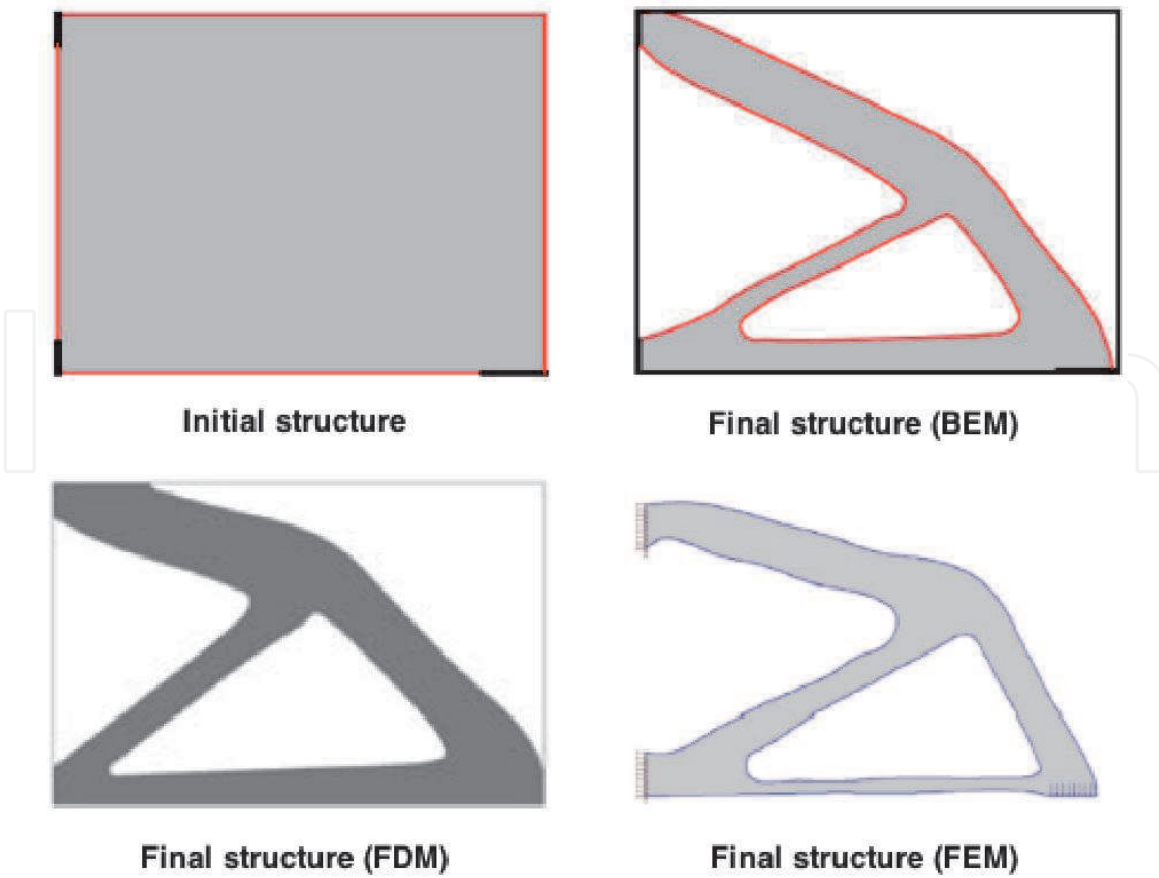
Figure 4.
Final cantilever beam structure for BEM, FDM and FEM.

	FDM	FEM	BEM
Number of Nodes	24000	27000	77
Number of Elements	8850	9650	40
CPU-Time [min.]	120	130	2
Memory [MByte]	75	85	0.4
Disc Space [MByte]	130	150	0
Accuracy of Results [%]	2.1	2.4	1.4

Table 1.
Comparison of computer resources needed for FDM, FEM and BEM modeling of cantilever beam structure.

illustrated in **Figure 6**. The BEM grid is composed of 76 nodes along *x* direction, and 51 nodes along *y* direction. This grid density was obtained after convergence analysis.

Figure 7 shows the cantilever beam optimization process from initial to final structure for different iterations.

The optimization results of the second example obtained with the proposed BEM are compared in **Figure 8** with FDM optimization results [71] and FEM optimization results of COMSOL Multiphysics software, version 5.4. It is clear from this figure that our BEM results obtained by the proposed technique are in excellent agreement with the FDM and FEM results.
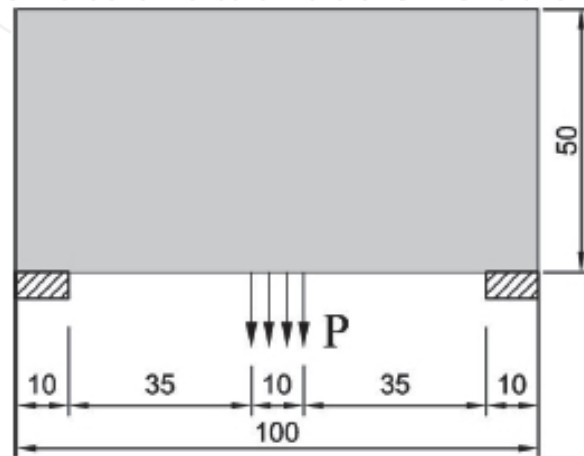

Figure 5.
Michel-type structure geometry.

Figure 6.
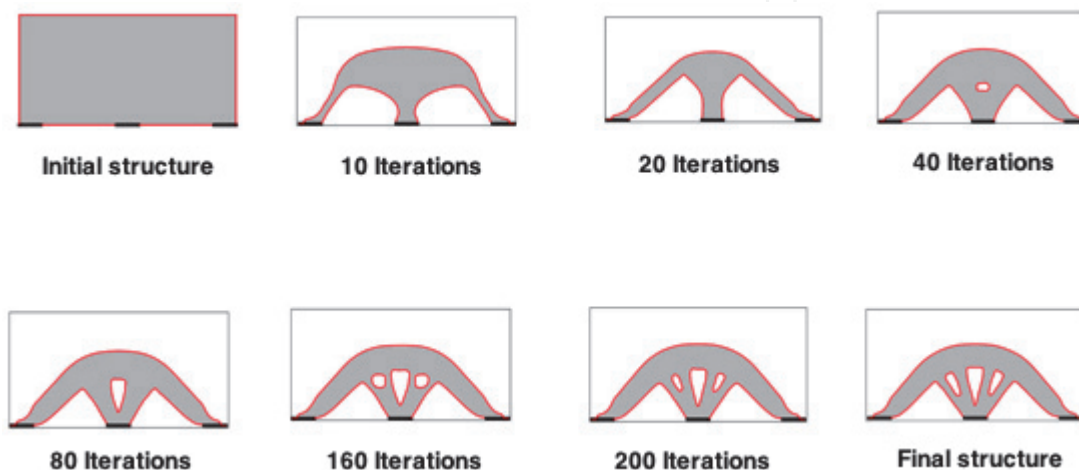*Initial boundary of the Michel-type structure.*

Figure 7.
Michell-type structure optimization process from initial to final structure for different iterations.

Table 2 shows that our proposed BEM modeling of Michell-type structure dramatically reduces the computer resources necessary to calculate our proposed modeling in comparison with the calculated results based on the FDM and FEM.
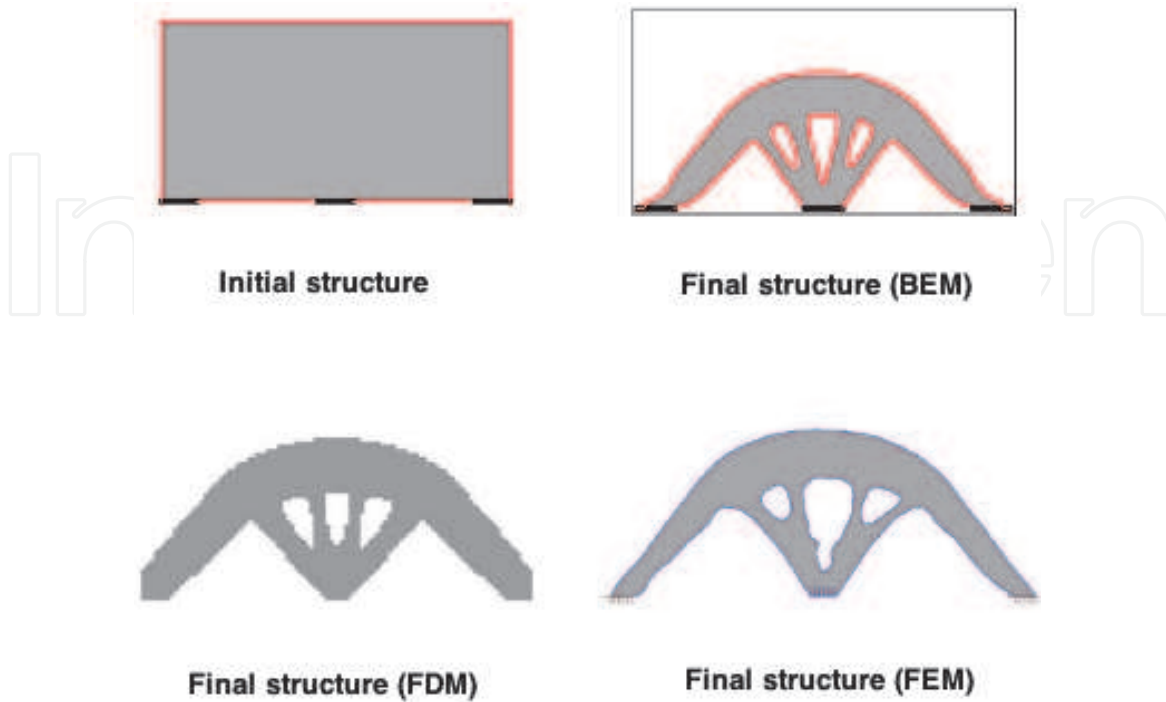

Figure 8.
Final Michell-type structure for BEM, FDM and FEM.

	FDM	FEM	BEM
Number of Nodes	26000	28000	30
Number of Elements	8950	9850	30
CPU-Time [min.]	130	140	2
Memory [MByte]	80	90	0.5
Disc Space [MByte]	160	180	0
Accuracy of Results [%]	2.2	2.5	1.5

Table 2.
Comparison of computer resources needed for FDM, FEM and BEM modeling of Michell-type structure.

6. Conclusion

In the present paper, we propose a new theory called nonlinear micropolar thermoviscoelasticity involving three temperatures. A new mathematical modeling of nonlinear generalized micropolar thermoviscoelasticity problem. A new boundary element technique for simulation and optimization problems of mechanics of solid deformable bodies is implemented based on genetic algorithm (GA), free form deformation (FFD) method and nonuniform rational B-spline curve (NURBS) as the global optimization technique for solving complex simulation and optimization problems associated with the proposed theory. FFD is an efficient and versatile parameterization technique for treating shape optimization problems with complex shapes. It is implemented for simulation and optimization of the shape. In the formulation of the considered problem, solutions are obtained for specific arbitrary parameters which are the control points positions in the considered problem, the profiles of the considered objects are determined by FFD method, where the FFD control points positions are treated as genes, and then the chromosomes profiles are defined with the genes sequence. The population is founded by a number of individuals (chromosomes), where the objective functions of individuals are determined by the boundary element method (BEM). Due to the large amount of computer resources required by the FDM and FEM, our proposed BEM model can be applied to a wide range of simulation and optimization problems related with our proposed theory. The numerical results demonstrate the validity, accuracy and efficiency of our proposed technique.

Nomenclature

$\alpha, \overline{\alpha}, \overline{\overline{\alpha}}, \breve{\alpha}$	micro-polar constants
β_{ij}	stress–temperature coefficients
δ_{ij}	Kronecker delta $(i, j = 1, 2)$
δ, η	weight coefficients
ε_{ij}	strain tensor
ε_{ijk}	alternate tensor
ϵ_{ij}	micro-strain tensor
λ	tractions
ϑ_0	viscoelastic relaxation time
ϖ	weights of control points
ρ	material density
σ_{ij}	force stress tensor
σ_0	reference stress
τ	time
τ_0, τ_1, τ_2	relaxation times
ω_i	micro-rotation vector
$\aleph$	$= \left(1 + \vartheta_0 \frac{\partial}{\partial \tau}\right)$ viscoelastic constant
b	internal heat generation vector
c	specific heat capacity
C_{ijkl}	constant elastic moduli
e	$= \varepsilon_{kk} = \epsilon_{kk}$ dilatation
$\mathbb{e}_{lij}$	piezoelectric tensor
F_i	mass force vector
J	micro-inertia coefficient
$\mathbb{J}$	current density vector

$\mathbb{K}_e$	electron conductive coefficients
$\mathbb{K}_i$	ion conductive coefficients
$\mathbb{K}_r$	phonon conductive coefficients
k, l	boundary points
M, N	sensors numbers
M_i	mass couple vector
m_{ij}	couple stress tensor
P	total energy of unit mass
P_e	$= c_e T_e$ Electron energy
P_i	$= c_i T_i$ Ion energy
P_r	$= \frac{1}{\rho} c_r T_r^4$ Phonon energy
$\mathbb{P}$	values vector of tractions and couple stress
$\mathrm{P_i}$	singular points
Q	heat flux vectors
$\mathbb{Q}$	values vector of displacements and microrotations
R	problem's boundary
S	problem's domain
T_e	electron temperature
T_i	ion temperature
T_r	phonon temperature
u	boundary displacement
u_i	displacement vector
u_0	reference displacement
u^k	computed displacements
$\hat{u}^k$	measured displacements
$\mathbb{W}_{ei}$	electron-ion energy coefficient
$\mathbb{W}_{er}$	electron–phonon energy coefficient

Author details

Mohamed Abdelsabour Fahmy
Faculty of Computers and Informatics, Suez Canal University, Ismailia, Egypt

*Address all correspondence to: mohamed_fahmy@ci.suez.edu.eg

IntechOpen

References

[1] Duhamel J. Some memoire sur les phenomenes thermo-mechanique. Journal de l'École Polytechnique. 1837;**15**:1-57

[2] Neumann F. Vorlesungen Uber die theorie der elasticitat. Brestau: Meyer; 1885

[3] Biot M. Thermoelasticity and irreversible thermo-dynamics. Journal of Applied Physics. 1956;**27**:249-253

[4] Lord HW, Shulman Y. A generalized dynamical theory of thermoelasticity. Journal of the Mechanics and Physics of Solids. 1967;**15**:299-309

[5] Green AE, Lindsay KA. Thermoelasticity. Journal of Elasticity. 1972;**2**:249-253

[6] Green AE, Naghdi PM. On undamped heat waves in an elastic solid. Journal of Thermal Stresses. 1992;**15**: 253-264

[7] Green AE, Naghdi PM. Thermoelasticity without energy dissipation. Journal of Elasticity. 1993; **31**:189-208

[8] Hetnarski RB, Ignaczak J. Soliton-like waves in a low-temperature nonlinear thermoelastic solid. International Journal of Engineering Science. 1996;**34**: 1767-1787

[9] Tzou DY. A unified approach for heat conduction from macro to micro scales. ASME Journal of Heat Transfer. 1995;**117**:8-16

[10] Tzou DY. The generalized lagging response in small-scale and high-rate heating. International Journal of Heat and Mass Transfer. 1995;**38**:3231-3240

[11] Tzou DY. Macro-to Microscale Heat Transfer: The Lagging Behavior. New York: Taylor & Francis; 1997

[12] Chandrasekharaiah DS. Hyperbolic thermoelasticity: A review of recent literature. Applied Mechanics Reviews. 1998;**51**:705-729

[13] Choudhuri SKR. On a thermoelastic three-phase-lag model. Journal of Thermal Stresses. 2007;**30**:231-238

[14] Chen PJ, Gurtin ME. On a theory of heat conduction involving two temperatures. Zeitschrift für Angewandte Mathematik und Physik. 1968;**19**:614-627

[15] Youssef H. Theory of two-temperature generalized thermoelasticity. IMA Journal of Applied Mathematics. 2006;**71**:383-390

[16] Fahmy MA. A new boundary element strategy for modeling and simulation of three-temperature nonlinear generalized micropolar-magneto-thermoelastic wave propagation problems in FGA structures. Engineering Analysis with Boundary Elements. 2019;**108**:192-200

[17] Eringen AC, Suhubi ES. Nonlinear theory of simple micro-elastic solid-I. International Journal of Engineering Science. 1964;**2**:189-203

[18] Eringen AC. Linear theory of micropolar elasticity. Journal of Mathematics and Mechanics. 1966;**15**: 909-923

[19] Tauchert TR Jr, Claus WD, Ariman T. The linear theory of micropolar thermoelasticity. International Journal of Engineering Science. 1968;**6**:36-47

[20] Eringen AC. Foundation of Micropolar Thermoelasticity, Courses and Lectures No. 23. Wein, Vienna: CISM International Centre for Mechanical Sciences/Springer-Verlag; 1970

[21] Tauchert TR. Thermal stresses in micropolar elastic solids. Acta Mech. 1971;**11**:155-169

[22] Dhaliwal RS. The steady-state axisymmetric problem of micropolar thermoelasticity. Archives of Mechanics. 1971;**23**:705-714

[23] Nowacki W, Olszak W. Micropolar Thermoelasticity. Wien, Vienna: CISM International Centre for Mechanical Sciences/Springer-Verlag; 1974

[24] Hetnarski RB, Eslami MR. Thermal Stresses—Advanced Theory and Applications. Netherlands: Springer-Verlag; 2008

[25] Eringen AC. Foundations of Micropolar Thermoelasticity. International Centre for Mechanical Sciences Book Series. Wien GMBH: Springer-Verlag; 1970

[26] Nowacki W. Couple-stresses in the theory of thermoelasticity. In: Proceedings IUTAM Symposia on Irreversible Aspects of Continuum Mechanics and Transfer of Physical Characteristics in Moving Fluids. Springer; 1968. pp. 259-278

[27] Marin M. On existence and uniqueness in thermoelasticity of micropolar bodies. Comptes Rendus de l'Académie des Sciences - Series I - Mathematics;**1995321**:475-480

[28] Ciarletta M. A theory of micropolar thermoelasticity without energy dissipation. Journal of Thermal Stresses. 1999;**22**:581-594

[29] Chirila A, Agarwal RP, Marin M. Proving uniqueness for the solution of the problem of homogeneous and anisotropic micropolar thermoelasticity. Boundary Value Problems. 2017;**2017**:3

[30] Nie C, Yu H. A Raviart–Thomas mixed finite element scheme for the two-dimensional three-temperature heat conduction problems. International Journal for Numerical Methods in Engineering. 2017;**111**:983-1000

[31] Hu Q, Zhao L. Domain decomposition preconditioners for the system generated by discontinuous Galerkin discretization of 2D-3T heat conduction equations. Communications in Computational Physics. 2017;**22**: 1069-1100

[32] Yi CZ, Zhang XW, Yan HX, Jin B. Finite element simulation and the application of amphoteric pH-sensitive hydrogel. International Journal of Applied Mechanics. 2017;**9**:1750063

[33] Eskandari AH, Baghani M, Sohrabpour S. A time-dependent finite element formulation for thick shape memory polymer beams considering shear effects. International Journal of Applied Mechanics. 2018;**10**:1850043

[34] Taghizadeh DM, Darijani H. Mechanical behavior modeling of hyperelastic transversely isotropic materials based on a new polyconvex strain energy function. International Journal of Applied Mechanics. 2018;**10**: 1850104

[35] Haghighat AE, Binesh SM. Domain decomposition algorithm for coupling of finite element and boundary element methods. Arabian Journal for Science and Engineering. 2014;**39**:3489-3497

[36] Fahmy MA. Boundary element algorithm for modeling and simulation of dual-phase lag bioheat transfer and biomechanics of anisotropic soft tissues. International Journal of Applied Mechanics. 2018;**10**:1850108

[37] Fahmy MA. Thermoelastic stresses in a rotating non- homogeneous anisotropic body. Numerical Heat Transfer, Part A: Applications. 2008;**53**: 1001-1011

[38] Fahmy MA, El-Shahat TM. The effect of initial stress and inhomogeneity on the thermoelastic stresses in a rotating anisotropic solid. Archive of Applied Mechanics. 2008;**78**: 431-442

[39] Fahmy MA. A time-stepping DRBEM for magneto-thermo-viscoelastic interactions in a rotating nonhomogeneous anisotropic solid. International Journal of Applied Mechanics. 2011;**3**:1-24

[40] Fahmy MA. A time-stepping DRBEM for the transient magneto-thermo-visco-elastic stresses in a rotating non-homogeneous anisotropic solid. Engineering Analysis with Boundary Elements. 2012;**36**:335-345

[41] Fahmy MA. Transient magneto-thermoviscoelastic plane waves in a non-homogeneous anisotropic thick strip subjected to a moving heat source. Applied Mathematical Modelling. 2012;**36**:4565-4578

[42] Fahmy MA. Numerical modeling of transient magneto-thermo-viscoelastic waves in a rotating nonhomogeneous anisotropic solid under initial stress. International Journal of Modeling, Simulation and Scientific Computing. 2012;**3**:1250002

[43] Fahmy MA. The effect of rotation and inhomogeneity on the transient magneto-thermoviscoelastic stresses in an anisotropic solid. ASME Journal of Applied Mechanics. 2012;**79**:1015

[44] Fahmy MA. Transient magneto-thermo-viscoelastic stresses in a rotating nonhomogeneous anisotropic solid with and without a moving heat source. Journal of Engineering Physics and Thermophysics. 2012;**85**:950-958

[45] Fahmy MA. Transient magneto-thermo-elastic stresses in an anisotropic viscoelastic solid with and without moving heat source. Numerical Heat Transfer, Part A: Applications. 2012;**61**: 547-564

[46] Fahmy MA. Implicit-explicit time integration DRBEM for generalized magneto-thermoelasticity problems of rotating anisotropic viscoelastic functionally graded solids. Engineering Analysis with Boundary Elements. 2013; **37**:107-115

[47] Fahmy MA. Generalized magneto-thermo-viscoelastic problems of rotating functionally graded anisotropic plates by the dual reciprocity boundary element method. Journal of Thermal Stresses. 2013;**36**:1-20

[48] Fahmy MA. A three-dimensional generalized magneto-thermo-viscoelastic problem of a rotating functionally graded anisotropic solids with and without energy dissipation. Numerical Heat Transfer, Part A: Applications. 2013;**63**: 713-733

[49] Fahmy MA. Boundary element modeling and simulation of biothermomechanical behavior in anisotropic laser-induced tissue hyperthermia. Engineering Analysis with Boundary Elements. 2019;**101**: 156-164

[50] Fahmy MA. A computerized DRBEM model for generalized magneto-thermo-visco-elastic stress waves in functionally graded anisotropic thin film/substrate structures. Latin American Journal of Solids and Structures. 2014;**11**:386-409

[51] Fahmy MA. A new LRBFCM-GBEM modeling algorithm for general solution of time fractional order dual phase lag bioheat transfer problems in functionally graded tissues. Numerical Heat Transfer, Part A: Applications. 2019;**75**:616-626

[52] Fahmy MA. Design optimization for a simulation of rotating anisotropic viscoelastic porous structures using time-domain OQBEM. Mathematics and Computers in Simulation. 2019;**66**: 193-205

[53] Fahmy MA. Shape design sensitivity and optimization for two-temperature generalized magneto-thermoelastic problems using time-domain DRBEM. Journal of Thermal Stresses. 2018;**41**: 119-138

[54] Fahmy MA. The effect of anisotropy on the structure optimization using golden-section search algorithm based on BEM. Journal of Advances in Mathematics and Computer Science. 2017;**25**:1-18

[55] Fahmy MA. DRBEM sensitivity analysis and shape optimization of rotating magneto-thermo-viscoelastic FGA structures using golden-section search algorithm based on uniform bicubic B-splines. Journal of Advances in Mathematics and Computer Science. 2017;**25**:1-20

[56] Fahmy MA. A predictor-corrector time-stepping DRBEM for shape design sensitivity and optimization of multilayer FGA structures. Transylvanian Review. 2017;**XXV**: 5369-5382

[57] Fahmy MA. Computerized Boundary Element Solutions for Thermoelastic Problems: Applications to Functionally Graded Anisotropic Structures. Saarbrücken, Germany: LAP Lambert Academic Publishing; 2017

[58] Fahmy MA. Modeling and optimization of anisotropic viscoelastic porous structures using CQBEM and moving asymptotes algorithm. Arabian Journal for Science and Engineering. 2019;**44**:1671-1684

[59] Fahmy MA. Boundary Element Computation of Shape Sensitivity and Optimization: Applications to Functionally Graded Anisotropic Structures. Saarbrücken, Germany: LAP Lambert Academic Publishing; 2017

[60] Fahmy MA. Shape design sensitivity and optimization of anisotropic functionally graded smart structures using bicubic B-splines DRBEM. Engineering Analysis with Boundary Elements. 2018;**87**:27-35

[61] Sladek V, Sladek J. Boundary element method in micropolar thermoelasticity. Part I: Boundary integral equations. Engineering Analysis. 1985;**2**:40-50

[62] Sladek V, Sladek J. Boundary element method in micropolar thermoelasticity. Part II: Boundary integro-differential equations. Engineering Analysis. 1985;**2**:81-91

[63] Sladek V, Sladek J. Boundary element method in micropolar thermoelasticity. Part III: Numerical solution. Engineering Analysis. 1985;**2, 2**:155-162

[64] Huang FY, Liang KZ. Boundary element method for micropolar thermoelasticity. Engineering Analysis with Boundary Elements. 1996;**17**:19-26

[65] Goldberg DE. Genetic Algorithms in Search, Optimization and Machine Learning. USA: Addison-Wesley Longman Publishing Co.; 1989

[66] Weile DS, Michielssen E. Genetic algorithm optimization applied to electromagnetics: A review. IEEE Transactions on Antennas and Propagation. 1997;**45**:343-353

[67] Janna C, Ferronato M, Sartoretto F, Gambolati G. FSAIPACK: A software package for high-performance factored sparse approximate inverse preconditioning. ACM Transactions on Mathematical Software. 2015;**41**:10: 1-10:26

[68] Eringen AC. Theory of micropolar elasticity. In: Liebowitz H, editor. Fracture. New York: Academic Press; 1968. pp. 621-729

[69] Dragos L. Fundamental solutions in micropolar elasticity. International Journal of Engineering Science. 1984;**22**: 265-275

[70] Oliveira HL, Leonel ED. Boundary element method applied to topology optimization using the level set method and an alternative velocity regularization. Meccanica. 2019;**54**: 549-563

[71] Itzá R, Viveros UI, Parra JO. Optimal implicit 2-D finite differences to model wave propagation in poroelastic media. Geophysical Journal International. 2016;**206**:1111-1125